ACS APPLIED MATERIALS & INTERFACES

Research Article

www.acsami.org

Printable Highly Conductive Conjugated Polymer Sensitized ZnO NCs as Cathode Interfacial Layer for Efficient Polymer Solar Cells

Jian Liu,[†] Jiang Wu,[†] Shuyan Shao,[‡] Yunfeng Deng,[†,§] Bin Meng,[†,§] Zhiyuan Xie,*[,†] Yanhou Geng,[†] Lixiang Wang,[†] and Fengling Zhang[‡]

[†]State Key Laboratory of Polymer Physics and Chemistry, Changchun Institute of Applied Chemistry, Chinese Academy of Sciences, Changchun 130022, P. R. China

[‡]Biomolecular and Organic Electronics, Department of Physics, Chemistry and Biology, Linkoping University, 58183 Linkoping, Sweden

[§]University of Chinese Academy of Sciences, Beijing 100039, P. R. China

Supporting Information

ABSTRACT: We report a facile way to produce printable highly conductive cathode interfacial layer (CIL) for efficient polymer solar cells (PSCs) by sensitizing ZnO nanocrystals (NCs) with a blue fluorescent conjugated polymer, poly(9, 9-bis-(6′-diethoxylphosphorylhexyl) fluorene) (PFEP). Herein, PFEP plays dual distinctive roles in the composite. Firstly, PFEP chains can effectively block the aggregation of ZnO NCs, leading to uniform and smooth film during solution processing via assembly on ZnO NC surfaces through their pending phosphonate groups. Secondly, PFEP can greatly improve the conductivity of ZnO NCs by charge transfer doping, that is the charge transfer from the sensitizer driven by electron-chemical potential equilibrium, which could be even more pronounced under light illumination because of light excitation of PFEP sensitizer. The increased conductivity in ZnO-PFEP layer renders more efficient electron transport and extraction compared to pristine ZnO layer. This ZnO-PFEP CIL was successfully applied to PSCs based on three polymer donor systems with different band-gaps, and efficiency enhancements from 44 to 70% were observed compared to those PSCs with pristine ZnO CIL. The highest efficiency of 7.56% was achieved in P(IID-DTC):$PC_{70}BM$-based PSCs by using ZnO-PFEP film as CIL. Moreover, the enhanced conductivity due to the charge-transfer doping effect allows thick ZnO-PFEP film to be used as CIL in high-performance PSCs. Both the high conductivity and good film-forming properties of ZnO-PFEP CIL are favorable for large-scale printable PSCs, which is also verified by high-efficiency PSCs with ZnO-PFEP CIL fabricated using doctor-blading, a large-scale processing technique. The work provides an efficient printable cathode interfacial material for efficient PSCs.

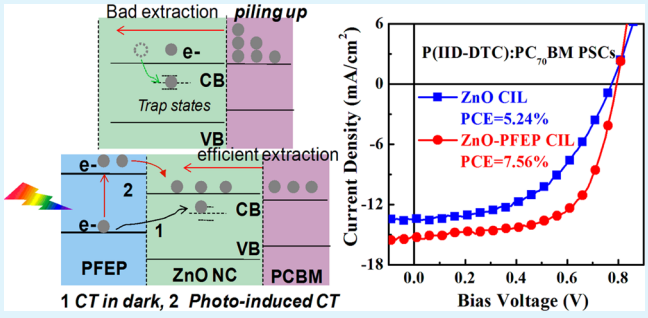

KEYWORDS: *polymer solar cells, cathode interfacial layer, ZnO nanocrystal, conductivity, sensitizer*

1. INTRODUCTION

Solution-processed polymer solar cell (PSC) is a promising candidate for inexpensive solar energy harvesting technologies due to its scalability, light weight and ease of low-temperature processing on flexible substrates.[1−3] High-efficiency PSCs commonly have a sandwich structure with an active layer comprising the conjugated polymer donor and fullerene derivative acceptor bulk heterojunction (BHJ) between two asymmetry electrodes.[4] In order to realize high photovoltaic conversion efficiency, it is required to utilize small band-gap donor for harvesting major fraction of solar photons, and finely tune the BHJ morphology of the active layer for efficient free charge generation and transport.[3,5−10] Besides the tailoring of the active layer, the interface engineering at the active layer/electrode contacts is equally important, which greatly influences the free charge extraction. For interfacial modification purpose, diverse interfacial layers have been used between the active layer and electrodes for delivering improved interfacial contacts.[11−13] Recently, the record laboratory power conversion efficiency (PCE) over 9% for the single-junction PSCs has been achieved by using a meticulously designed conjugated polymer as the cathode interfacial layer (CIL). For commercialization of PSCs, high-performance PSCs must be achieved with large-scale processing technology such as roll-to-roll (R2R) printing technology.[14,15] However, to date, most of interface studies have been focusing on improving device performance. The feasibility of fabricating these interfacial layers with large-scale processing strategies such as slot-die coating and doctor blading, etc., has rarely been concerned. Therefore, it is of crucial importance to develop efficient and

Received: February 17, 2014
Accepted: May 9, 2014
Published: May 20, 2014

   dx.doi.org/10.1021/am501001v | ACS Appl. Mater. Interfaces 2014, 6, 8237−8245

simultaneously printable interfacial layers for high-performance and low-cost PSCs.

The interfacial layers play very critical roles in high-efficiency PSCs such as offering favorable ohmic contacts with electrodes, eliminating charge recombination and serving as an optical spacer layer for light manipulation.[16−18] Alcohol/aqueous solution-processed CILs including alcohol-soluble conjugated polymers and inorganic metal oxides have been highly concerned in recent years.[19−24] The optimal thickness of polymeric CIL is merely a few of nanometers and thus limits its realization in practical large-area manufacturing. Colloidal zinc oxide (ZnO) nanocrystals (NCs) have been widely used as CIL because of its low work function, wide band gap, as well as the facile synthesis.[16,25,26] However, ZnO NCs film often suffers from poor morphology because of large-scale aggregation in solution-processing and surface trap-limited low electron transport. Very recently, aiming at improving the ZnO NCs film morphology, insulating poly(vinylpyrrolidone) (PVP) has been utilized to mediate the growth of ZnO NCs.[27] However, the conductivity of ZnO-PVP nanocomposite is greatly compromised due to the insulating nature of PVP, leading to poor fill factor (FF) for PSCs, and thereby UV-zone treatment is required to remove excess PVPs for recovering the photovoltaic performance. To improve the electron transport in ZnO NCs film, lattice doping strategy is usually used to produce n-doped films, such as Al-doped or Li-doped ZnO layer.[28−30] However, lattice doping technique needs high temperature to promote doped atoms into the lattice of ZnO, which is not compatible with flexible substrate. Moreover, those n-doped ZnO films do not show improved film morphology when processed from solutions.

Herein, we report a facile way to produce efficient printable CIL by sensitizing ZnO NCs with a blue fluorescent conjugated polymer, poly(9, 9-bis (6′-diethoxylphosphorylhexyl) fluorene) (PFEP). The phosphonate-functionalized groups in PFEP are prone to interact with ZnO NCs and allow PFEP molecules to easily assemble on ZnO NCs surface, leading to more uniform and smooth morphology. More interestingly, the carrier density in ZnO film is largely increased due to the charge transfer from PFEP sensitizer driven by electron-chemical potential equilibrium. This charge transfer doping effect could be even more catalysed by light because of blue light-absorbing nature of PFEP sensitizer. The increased carrier density in PFEP-sensitized ZnO layer renders it more efficient electron transport and extraction with respect to pristine ZnO layer. To generalize its application, ZnO-PFEP CIL is incorporated into PSCs based on three different polymer donor systems, and considerable efficiency enhancements from 44 to 70% are observed compared to those PSCs with pristine ZnO CIL. The highest efficiency of 7.56% is achieved in poly[*N*-dedocyldithieno[3,2-*b*;6,7-*b*]carbazole-*alt*-*N*,*N*′-(2-octyldodecanyl)-isoindigo (P-(IID-DTC)):$PC_{70}BM$-based PSCs with ZnO-PFEP CIL. Moreover, the results demonstrate that high-performance PSCs can be achieved with thick ZnO-PFEP CIL because of the enhanced conductivity. Both the high conductivity and good film-forming properties of ZnO-PFEP CIL are favorable for large-scale printable PSCs, which is also verified by high-efficiency PSCs with ZnO-PFEP CIL fabricated using doctor-blading, a large-scale film processing technique. This work provides an efficient printable cathode interfacial material for efficient PSCs.

2. EXPERIMENTAL SECTION

Materials. PCDTBT and P(IID-DTC) were synthesized in our laboratory. PDPP3T was purchased from Solarmer Material Inc., and $PC_{70}BM$ was purchased from American Dye Source. Inc. PFEP was synthesized in our laboratory following the reported method.[31] ZnO NCs with a diameter of 5 nm were prepared according to the synthesis route reported by Beek et al.[25] The ZnO NCs and PFEP with weight ratio of 6:1 were co-dissolved in n-butanol solvent, and stirred at 80 °C for at least 10 h until the solution was clear and blue, making sure the assembling process was completed.

Film Characterization. Atomic force microscopy (AFM) measurement was carried out in air using SPA 300HV with an SPI3800 controller, Seiko Instruments Industry, Co., Ltd. Absorption and photoluminescence (PL) spectra of the samples were taken using a PerkinElmer 35 UV-visible spectrophotometer. The refractive index (n and k values) of the films was measured using spectroscopic ellipsometry (Horiba Jobin Yvon). The thickness of various layers was measured with a Dektak 6M Stylus Profiler. The ultraviolet photoelectron spectroscopy (UPS) measurements were performed on Thermo ESCALAB 250 using He−I (21.2 eV) discharge lamp and a sample bias of −12 V for separating the sample and the secondary edge for the analyzer.

Conductivity and Mobility Measurement. The ZnO NCs and ZnO-PFEP layers with different thicknesses were sandwiched between ITO and Al electrode. The dark $J-V$ characteristics were tested with a Keithley 2400 source meter. The resistance values were extracted from dark $J-V$ characteristics. The conductivities of two types of CILs were obtained by fitting resistance-thickness curves. The photoconductivity of different layers were recorded under AM 1.5G irradiation with an intensity of 100 mW cm^{-2}. The electron-only devices were fabricated with a structure of ITO/Al/ZnO or ZnO-PFEP/Al. The mobilities (μ_e) were extracted by fitting experimental data using the following formula[32]

$$J = \frac{9}{8}\xi_r\xi_0\mu_e \exp\left(0.891\gamma_e\sqrt{\frac{V}{L}}\right)\frac{V^2}{L^3} \quad (1)$$

where ξ_r, ξ_0, and γ_e represent the relative dielectric constant of materials, vacuum dielectric constant, and field dependence factor of mobility, respectively. The schottky-junction devices were fabricated with a structure of ITO/PEDOT:PSS/ZnO NCs or ZnO-PFEP/Al. The PEDOT:PSS layer was ca. 80 nm and the ZnO NCs or ZnO-PFEP layer were ca. 100 nm.

Fabrication and Measurement of PSCs. Conventional solar cells were fabricated on ITO glass substrates. The ITO glass substrates were first cleaned with detergent, ultrasonicated in water, acetone, and isopropyl alcohol sequentially, and then dried at 120 °C in an oven overnight. PEDOT:PSS (Baytron 4083) was spin-cast on ITO substrate to form a 45 nm thick hole-transporting layer and dried at 120 °C for 30 min in an oven. Three respective solutions, containing a mixture of PCDTBT:$PC_{70}BM$ (1:4, w/w) in dichlorobenzene with a concentration of 20 mg mL^{-1}, a mixture of PDPP3T:$PC_{70}BM$ (1:2, w/w) in dichlorobenzene:chloroform:1, 8-diiodooctane (0.76:0.19:0.05, v/v/v) with a concentration of 24 mg mL^{-1} and mixture of P(IID-DTC):$PC_{70}BM$ (1:2, w/w) in dichlorobenzene with a concentration of 24 mg mL^{-1}, were spin-cast on top of the PEDOT:PSS layer to produce a 80 nm-thick PCDTBT:$PC_{70}BM$ layer, 120 nm thick PDPP3T:$PC_{70}BM$ layer and 130 nm thick P(IID-DTC):$PC_{70}BM$ layer. The different CILs were deposited upon the active layers by spin-coating from the pure PFEP, ZnO NCs and ZnO-PFEP n-butanol solutions. The varied thicknesses of the CILs were obtained by controlling the concentrations of solutions and spin-coating speeds. Then Al (80 nm) cathode was thermally deposited to complete the device fabrication. The active area of the cell was 12.5 mm^2, which was defined by the overlapping area of the ITO and Al electrodes and calibrated by the optical microscopy image. The photovoltaic cells were illuminated by a Newport 300W solar simulator with an AM 1.5G filter providing an intensity of 100 mW cm^{-2}. The light intensity was determined by a calibrated silicon diode with KG-5 visible color filter. The $J-V$ traces were obtained with a Keithley 236 source meter.

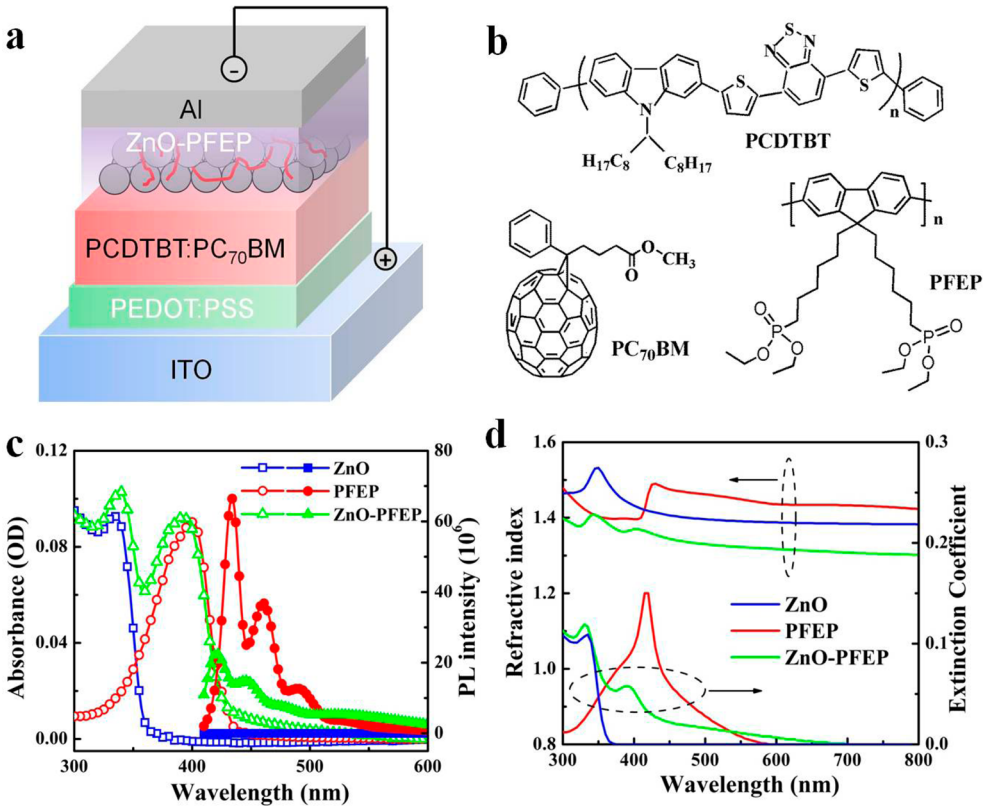

Figure 1. (a) Device architecture of polymer solar cells with hybrid ZnO-PFEP CIL; (b) molecular structures of PCDTBT, $PC_{70}BM$ and PFEP; (c) absorption and PL spectra of ZnO, PFEP and ZnO-PFEP films; (d) optical constants (n and k) of ZnO, PFEP, and ZnO-PFEP films.

External quantum efficiency (EQE) measurements were performed under short-circuit conditions with a lock-in amplifier (SR830, Stanford Research System) at a chopping frequency of 280 Hz during illumination with a monochromatic light from a xenon lamp.

3. RESULTS AND DISCUSSION

The device structure of PSCs studied in this work is shown in Figure 1a and the corresponding energy level alignment of the device is given in Figure S1 in the Supporting Information. The anode interfacial layer PEDOT:PSS, the PCDTBT:$PC_{70}BM$ blend active layer and ZnO-PFEP hybrid CIL were deposited sequentially via simple solution-processing method (see the details in Experimental Section). The molecular structures of PCDTBT, $PC_{70}BM$ and PFEP are shown in Figure 1b. Because the morphological and electrical behavior of the CIL has been proved to be very crucial to the performance of PSCs, we firstly investigated the properties of hybrid ZnO-PFEP film with respect to pristine ZnO NCs and then explored its application in PSCs. The absorption and PL spectra of pristine ZnO, PFEP and ZnO-PFEP films are depicted in Figure 1c. The absorption spectrum of the ZnO-PFEP layer was nearly superimposition of the pure ZnO and PFEP films with the peak assigned to PFEP constituent slightly blue-shift with respect to its pure film. In PL spectra, strong PL quenching of PFEP by ZnO NCs was observed in PFEP sensitized ZnO film, which indicated the occurrence of photo-induced electron transfer from PFEP molecules to ZnO NCs. It was assumed that in ZnO-PFEP film, PFEP sensitizer likely serves as electron donor with lowest unoccupied molecular orbital (LUMO) level of −2.3 eV and highest occupied molecular orbital (HOMO) level of −5.3 eV, and ZnO NCs as electron acceptor with conduction band (CB) edge and valence band (VB) edge of −4.1 and −7.5 eV, respectively.[33,34] In addition to the strong PL quenching of PFEP in ZnO-PFEP film, blue shift of PFEP PL emission was clearly observed compared to its pure film. It has been disclosed that the emission characteristics of PF family can be greatly influenced by the morphology of their solid states.[35,36] For the pure PFEP film, the emission peaks locate at 434 nm (0-0 band) and 460 nm (0-1 band), which are assigned to typical emission feature of crystalline α-phase of PF backbone.[33] As for the ZnO-PFEP film, the emission peaks are at 421 nm (0-0 band) and 447 nm (0-1 band), indicating the PFEP were more amorphous due to introduction of ZnO NCs. This change is resulted from the interaction between ZnO NCs and phosphonate groups on PFEP chains. Consequently, PFEP chains are randomly dispersed within the ZnO NCs matrix and the intra- and inter-chain packing are severely disturbed. In Figure 1d, the optical constants (refractive index and extinction coefficient) of various films are displayed. In comparison to pristine ZnO NCs film, the refractive index of ZnO-PFEP film is distinctly reduced, indicating that the ZnO NCs in the hybrid film become less aggregated after incorporating PFEP constituent. The flexible PFEP chains might serve as plasticizer in rigid ZnO film, and impart the ZnO-PFEP film improved mechanical flexibility compared to closely packed ZnO NCs film. The increased flexibility will render such hybrid CIL being more suitable for R2R-processed "plastic" PSCs.

The surface topographies of the pristine ZnO NCs and ZnO-PFEP film were investigated by AFM and the corresponding results are shown in Figure 2. As observed in Figure 2a, the ZnO NCs were prone to form large aggregates and rough surface with root mean square (RMS) roughness of 4.2 nm. In contrast, the aggregation of ZnO NCs in hybrid ZnO-PFEP film (Figure 2b) was significantly restrained and consequently

dx.doi.org/10.1021/am501001v | ACS Appl. Mater. Interfaces 2014, 6, 8237−8245

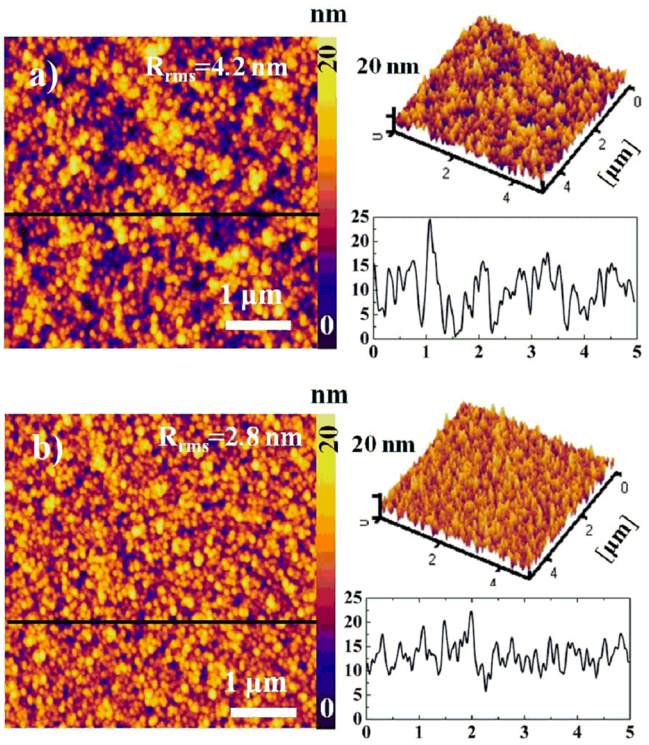

Figure 2. 2D and 3D topographicaphic AFM images and the surface profiles of (a) the pure ZnO NCs and (b) hybrid ZnO-PFEP films.

the surface became smoother with less RMS roughness of 2.1 nm. Such an improvement is attributed to the potential interaction between ZnO NCs and phosphonate-functionalized groups on PFEP, resulting in a more uniform film.[37] This argument is also supported by the decreased refractive index because increasing the distance among ZnO NCs would decrease its refractive index.[38]

Figure 3a displays the resistance (R) values of the ZnO NCs and ZnO-PFEP films at different thicknesses. The R values were extracted by sandwiching the films between transparent ITO and Al as shown in the inset. The ZnO-PFEP film distinctly exhibited higher conductivity than the pristine ZnO NCs film. After sensitizing by PFEP, the conductivity of ZnO-PFEP film was increased by nearly two folds compared to that of pristine ZnO NCs. This finding is significantly contrary to the previously reported ZnO-PVP blend, where the insulating PVP blocked electron transport among ZnO NCs and thus decreased the conductivity of the resulted film.[27] The zero-field electron mobilities of pristine ZnO NCs and ZnO-PFEP films were extracted from their electron-only devices as shown in Figure 3b. The hybrid film displayed an electron mobility of 7.89×10^{-3} cm^2 (V s)$^{-1}$, which was slightly lower with respect to 8.42×10^{-3} cm^2 (V s)$^{-1}$ for the pristine ZnO NCs film. However, as shown in the inset of Figure 3b, the double logarithm current density–voltage (J–V) characteristics of the two electron-only devices displayed different features in the low bias regime. A transition of the slope from 1 to 2 was observed for the pristine ZnO NCs-based device, whereas the slope kept constant with a value of 1 at small bias regime for the ZnO-

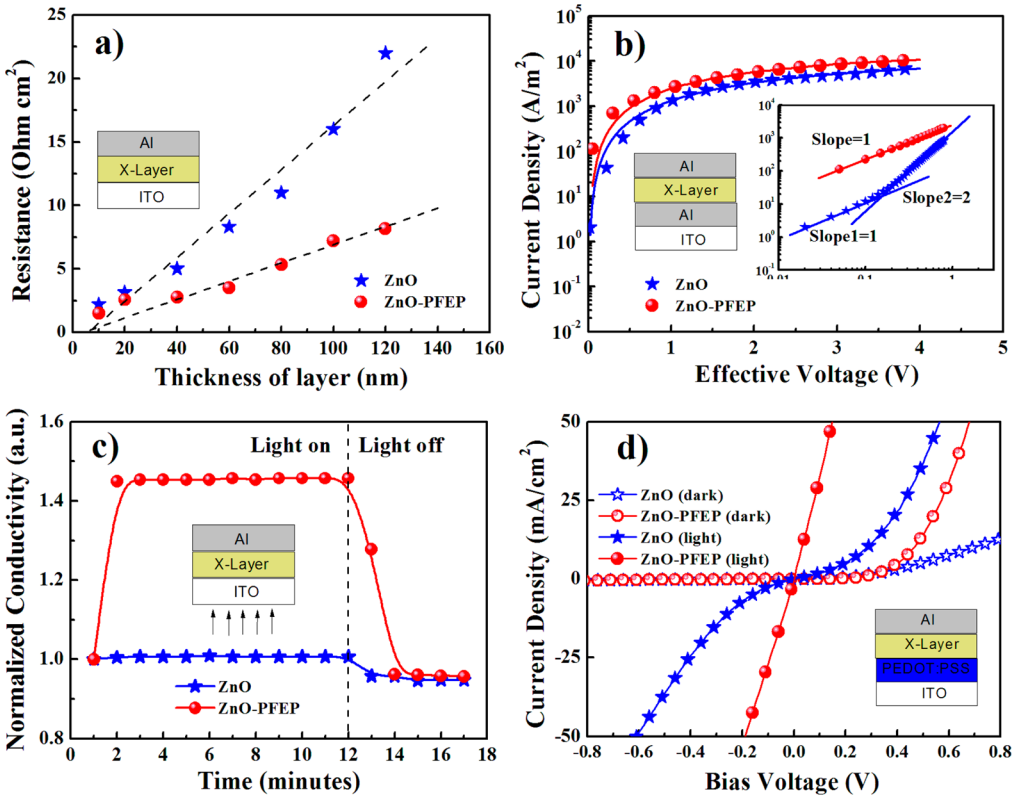

Figure 3. (a) Resistance of ZnO and ZnO-PFEP films with varied thicknesses; (b) J–V characteristics of the electron-only devices with the ZnO (140 nm) and ZnO-PFEP (110 nm) layers, the inset is the corresponding double logarithm J–V curves under small bias region; (c) photoconductivity response of the ZnO and ZnO-PFEP films with the same thickness of 80 nm; (d) dark and illuminated J–V characteristics of schottky-junction devices based on ZnO NCs and ZnO-PFEP layers on metallic PEDOT:PSS layer. The corresponding device architectures are shown in the insets.

dx.doi.org/10.1021/am501001v | ACS Appl. Mater. Interfaces 2014, 6, 8237–8245

PFEP based device. The slope transition implies that the concentration of injected electrons exceeded the intrinsic electron concentration, and hence the space charge limited current was dominated in the film.[39,40] The discrepancy in slope variations of two samples implied that the number of thermally generated electrons in ZnO-PFEP film is increased compared to the pristine ZnO film, rendering ZnO-PFEP film more conductive nature under small bias. This increased electron concentration in hybrid ZnO-PFEP film accounts for the conductivity enhancement even though the electron mobility is slightly reduced. It is proposed that the increased electron population may be a result of the charge transfer between PFEP species and ZnO NCs, which will be further validated later.

Figure 3c displays the normalized conductivities of ZnO and ZnO-PFEP films in dark and under AM 1.5G 100 mW cm^{-2} irradiation at different times. As can be seen, both the two films exhibited distinctive photo-conductivity behaviour with the photo-conductivity being largely increased after PFEP incorporation. The photo-conductivity behaviour of ZnO NCs has been investigated previously and it is found that the gradual release of trapped electrons by chemisorbed oxygen and simultaneous electron accumulation on CB states upon UV light soaking contribute to the increased conductivity.[41−43] However, such trap-released mechanism is not able to account for the increased photoconductivity in hybrid ZnO-PFEP film due to the more increased conductivity of hybrid ZnO-PFEP film in regard to the pure ZnO film. It is assumed that photo-excitation of PFEP and subsequent photo-induced charge transfer to ZnO NCs may occur in ZnO-PFEP blend film. This photo-induced electron transfer process largely increases the electron concentration on the CB of ZnO NCs, thereby increasing the conductivity. This kind of interfacial layer with high conductivity under illumination is favorable for reducing series resistance and facilitating electron extraction for PSCs. The increased electron concentration in hybrid ZnO-PFEP film layer in dark and under light soaking is further verified with the schottky-junction devices with the n-type ZnO NCs or ZnO-PFEP films sandwiched between the high work-function PEDOT:PSS anode and Al cathode. The electrical property of such schottky-junction devices is primarily dominated by the triangular barrier width at the PEDOT:PSS/ZnO or ZnO-PFEP interfaces, which is strongly dependent on the electron concentration in the semiconductor layer.[44] Figure 3d displays the $J-V$ characteristics of two types of schottky-junction devices in dark and under light soaking. In dark, the electron concentrations in both samples are not sufficiently high and the resultant large barrier widths render them diode behaviour. The ZnO-PFEP hybrid layer based device exhibits relatively narrow barrier compared to pristine ZnO NCs based device, implying the increased electron concentration in hybrid ZnO-PFEP layer. Upon light soaking, both devices show resistive behavior especially for the ZnO-PFEP-based device, indicating that the electron concentration in both films were greatly increased and the energy barriers are significantly thin enough for electrons to tunnel through.

Different from the common n-type doping in organic semiconductors,[45] the conductivity enhancement of the ZnO-PFEP film is attributed to the following two aspects. Firstly, the phosphonate groups in PFEP chains contain oxygen atoms bearing with lone pair electrons which are prone to interact with zinc atom on the surface of NCs, providing an electron-potential offset.[46] The electrons are driven from PFEP to ZnO by this electron-potential offset. It has been verified that the charge exchange between transition metal oxides and organic semiconductors can be driven by the electron-chemical potential equilibrium.[47] The energy level alignment of the ZnO and ZnO-PFEP films to ITO electrode was characterized using UPS technique and the corresponding UPS spectra are shown in Figure 4. It is clearly seen that the Fermi level of

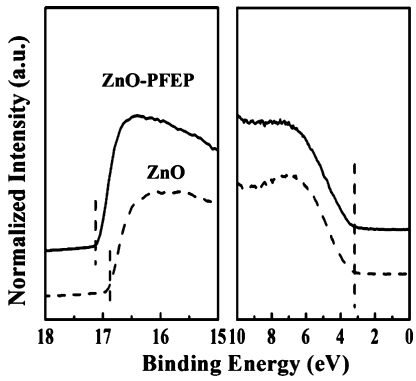

Figure 4. UPS spectra of ZnO NPs and hybrid ZnO-PFEP films on the ITO substrates.

ZnO-PFEP film moved upwards with 0.2 eV in regard to the pristine ZnO, indicating existence of ground-state electron transfer from PFEP to ZnO NCs. Second, the ZnO-PFEP possesses the photoinduced electron transfer feature as conjugated PFEP can absorb short-wavelength light, rendering the film high conductivity under solar light. It is highly expected that this PFEP-sensitized ZnO will be more suitable for high-efficiency PSCs to serve as the CIL compared to the ZnO NCs.

The PCDTBT:PC_{70}BM BHJ PSCs with the PFEP, ZnO, and ZnO-PFEP as the CILs were fabricated and the corresponding photovoltaic parameters of the devices with different-thickness CILs together with the series and shunt resistance (R_s and R_{sh}) variances are shown in Table 1. The illuminated $J-V$ characteristics for the PCDTBT:PC_{70}BM PSCs with 1 nm-thick PFEP, 25 nm thick ZnO and 25 nm thick ZnO-PFEP

Table 1. Photovoltaic Parameters of the PCDTBT:PC_{70}BM PSCs with Different Thickness of PFEP, ZnO NCs, and Hybrid ZnO-PFEP CILs under AM 1.5G 100 mW cm^{-2} Irradiation

devices	thickness (nm)	V_{OC} (V)	J_{SC} (mA cm^{-2})	FF	PCE (%)	R_{sh} (kΩ cm^2)	R_s (Ω cm^2)
PFEP	0.5	0.70	10.2	0.584	4.18	0.58	4.56
	1	0.88	10.6	0.649	6.05	0.68	3.96
	2	0.90	10.8	0.582	5.66	0.42	3.50
	3	0.90	11.0	0.386	3.82	0.12	10.6
	5	0.80	9.55	0.202	1.54	0.06	22.4
ZnO	10	0.85	10.0	0.585	4.90	7.89	6.80
	25	0.89	10.3	0.516	4.08	4.39	14.0
	50	0.87	8.11	0.420	2.96	0.28	20.4
	75	0.87	6.20	0.231	1.25	0.17	26.8
	100	0.85	3.65	0.228	0.71	0.13	45.6
ZnO-PFEP	10	0.89	10.3	0.653	5.99	0.82	2.35
	25	0.91	10.8	0.705	6.93	1.74	2.40
	50	0.88	8.76	0.714	5.50	7.94	2.52
	75	0.87	7.30	0.681	4.33	1.61	2.58
	100	0.88	6.50	0.661	3.78	1.02	3.10

interfacial layers are displayed in Figure 5a and the illuminated $J-V$ characteristics of PSCs with different-thickness PFEP, ZnO

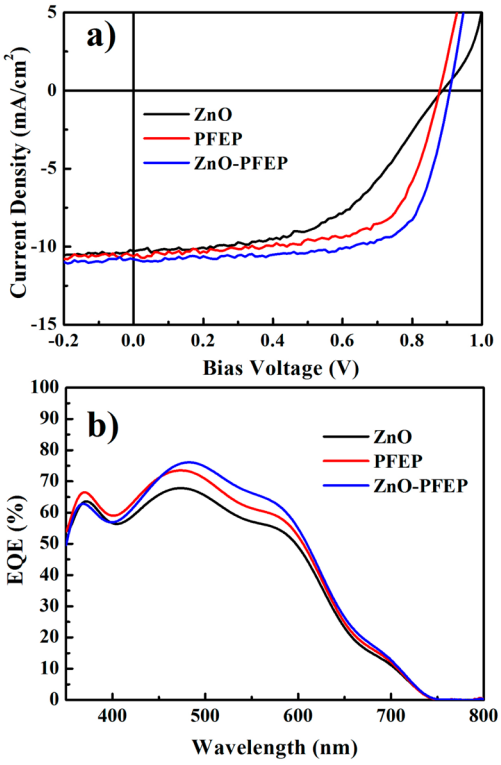

Figure 5. (a) Illuminated $J-V$ characteristics and (b) corresponding EQE spectra of PCDTBT:$PC_{70}BM$ PSCs with 1 nm PFEP, 25 nm ZnO, and 25 nm ZnO-PFEP CILs.

and ZnO-PFEP are shown in Figure S2 in the Supporting Information. The PCDTBT:$PC_{70}BM$ PSCs with pure PFEP as the CIL demonstrates a PCE of 6.05% with an optimal PFEP thickness of 1 nm. With increase of PFEP from 2 to 5 nm, the Rs is rapidly increased from 3.5 to 22.4 Ω cm^2. The PCDTBT:$PC_{70}BM$ PSC with 25 nm-thick ZnO CIL exhibited a PCE of 4.08% with a low FF of 51.6%, a short-circuit current density (J_{SC}) of 10.3 mA cm^{-2} and an open-circuit voltage (V_{OC}) of 0.89 V. The small FF value indicates that the electron extraction is inefficient because of the low conductivity of pristine ZnO CIL, leading to electron accumulation at the cathode interfaces and thereby bimolecular recombination at the region of low built-in electric field.[48,49] When the ZnO layer thickness is increased from 10 to 100 nm, the R_s of the resulted devices increases from 6.8 to 45.6 Ω cm^2, highlighting the low conductivity of ZnO CIL. With the PFEP sensitizing, the conductivity of ZnO-PFEP film was significantly enhanced, resulting in efficient electron extraction. Consequently, the solar cells with 25 nm-thick ZnO-PFEP CIL achieved an impressive FF of 70.5%, a J_{SC} of 10.8 mA cm^{-2}, a V_{OC} of 0.91 V, and an overall PCE of 6.93%, representing about 70% enhancement compared to that of ZnO NCs-based cells. The R_s merely increases from 2.35 to 3.10 Ω cm^2 when the ZnO-PFEP thickness is increased from 10 to 100 nm. The EQE spectra of the three solar cells are displayed in Figure 5b. The calculated J_{SC} values from EQE spectra are within 3% error compared to the measured J_{SC} values. The highest EQE peak of 75% was achieved for the PSCs with ZnO-PFEP interfacial layer, indicating the efficient photon-electron conversion.

Figure 6a plots the FF variance of the PCDTBT:$PC_{70}BM$ PSCs with different thicknesses of PFEP, ZnO, and ZnO-PFEP

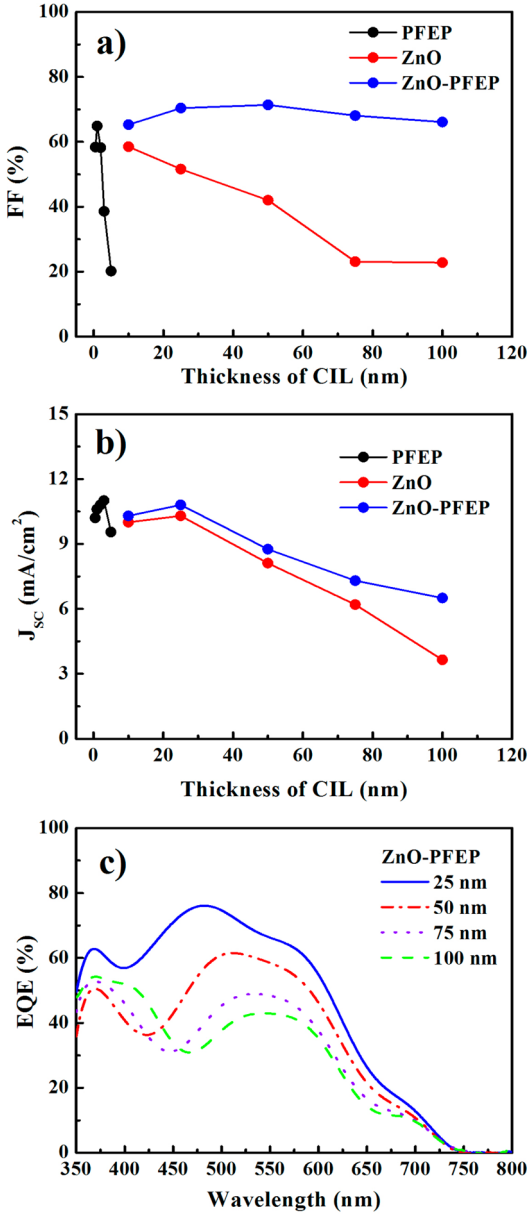

Figure 6. (a) FF and (b) J_{SC} values of the PCDTBT:$PC_{70}BM$ solar cells as a function of the thicknesses of PFEP, ZnO, and ZnO-PFEP CILs. (c) Corresponding EQE spectra of PSCs with different-thickness ZnO-PFEP CILs.

CILs, respectively. As can be seen, the FF of the PSCs with pure PFEP as the CIL shows a peak value of 64.9% at a PFEP thickness of ca. 1 nm and then declined rapidly to 20.2% with the PFEP thickness of CIL further increased to 5 nm. For the cells with ZnO as the CIL, when the ZnO thickness is increased from 10 to 100 nm, the FF value is gradually reduced from 58.5% to 22.8%. This phenomenon reflect that the conductivity of CIL strongly affect the electron extraction and thus FF of the cells as the increase of the thickness of low conductive CIL. Although a high FF of 64.9% is achieved for the PSCs with 1 nm PFEP, the 1 nm thick PFEP is almost unrealizable for current printing technologies. In contrast, by using the ZnO-PFEP with improved conductivity as the CIL, the FF reaches a

dx.doi.org/10.1021/am501001v | ACS Appl. Mater. Interfaces 2014, 6, 8237−8245

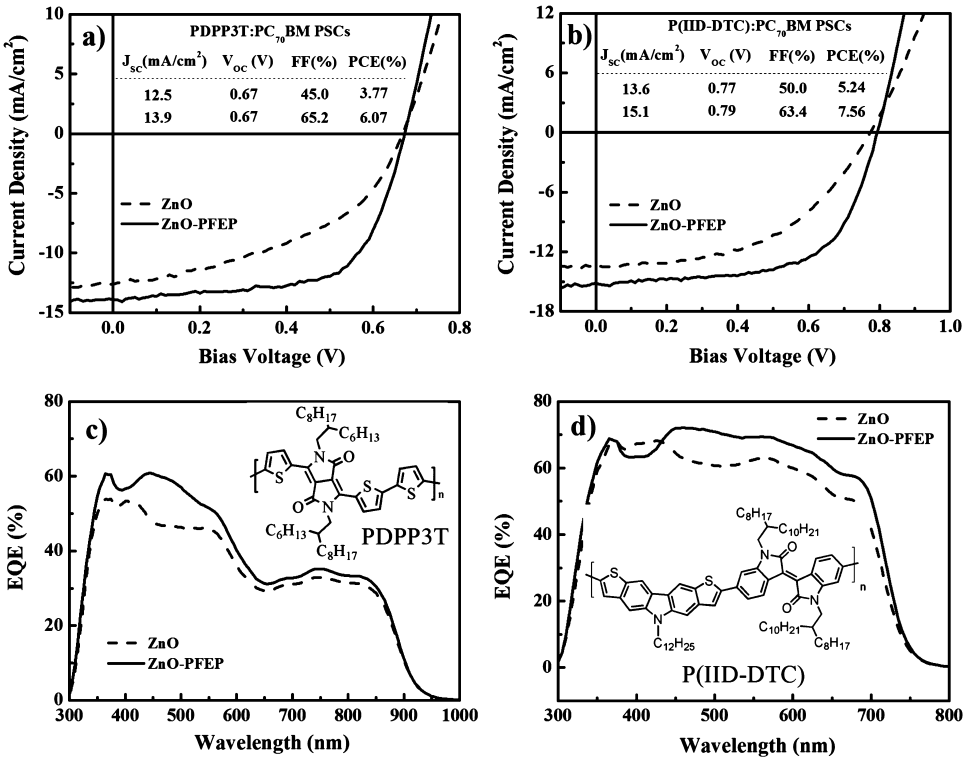

Figure 7. Illuminated *J*–*V* characteristics of PSCs based on (a) PDPP3T:$PC_{70}BM$ and (b) P(IID-DTC):$PC_{70}BM$ systems with ZnO and ZnO-PFEP films as CILs. The corresponding device performances are summarized in the insets of each panel. The EQE spectra of PSCs based on (c) PDPP3T:$PC_{70}BM$ and (d) P(IID-DTC):$PC_{70}BM$ systems with ZnO and ZnO-PFEP films as CILs. The molecular structures are shown in the insets of each panel.

peak value of 71.4% at a ZnO-PFEP thickness of 50 nm and even remains at 66% when the ZnO-PFEP thickness is up to 100 nm, which is more suitable for large-scale processing. Figure 6b plots the J_{SC} variance of the PCDTBT:$PC_{70}BM$ PSCs with different thicknesses of PFEP, ZnO and ZnO-PFEP CILs, respectively. Both of the PSCs with ZnO and ZnO-PFEP CILs show similar trend of J_{SC}, though the FFs of the two cells are quite different. With further increasing of CIL thickness from 25 to 100 nm, the J_{SC} of the cell gradually decrease. This variance can be attributed to the redistribution of absorption profile of incident solar light in the active layer, since the active layer is fixed at 80 nm. The EQE spectra of PSCs with hybrid ZnO-PFEP CIL shown in Figure 6c demonstrate red-shift EQE peak with the ZnO-PFEP thickness varied from 25 to 100 nm, which can be considered as a fingerprint of optical interference effects as the CIL thickness varied. Optical simulations were implemented on the PSCs with varying thickness ZnO-PFEP CILs as shown in Figure S3 in the Supporting Information. The modelling results indicated that the decreased J_{SC} in PSCs with thicker ZnO-PFEP CILs mainly resulted from optical spacer effect of ZnO-PFEP CIL. By increasing the active layer thickness, the J_{SC} could be recovered. When the active layer was increased up to 120 nm combined with 100 nm-thick ZnO-PFEP CIL, J_{SC} was increased to 10.3 mA cm^{-2} again, with impressive FF of 66% and overall PCE of 5.75% been achieved (see Figure S4 in the Supporting Information).

To explore the feasibility of general application in PSCs, we also extended the ZnO-PFEP CIL to the PSCs based on low-band-gap polymer systems, such as PDPP3T and P(IID-DTC), and the corresponding results are shown in Figure 7. High efficiencies of 6.07% and 7.56% were achieved using PFEP sensitized ZnO film as CIL in PDPP3T:$PC_{70}BM$ and P(IID-DTC):$PC_{70}BM$ based PSCs, representing 61% and 44% enhancement with respect to ZnO-based cells. The results indicated that the PFEP sensitized ZnO CIL might be universal for most of PSCs and could be used as solution-processed CIL in high-efficiency PSCs. In order to verify the possibility of printing the ZnO-PFEP in PSCs, the PSCs with the PEDOT:PSS anode interfacial layer, the PCDTBT:$PC_{70}BM$ active layer and ZnO-PFEP CIL prepared with doctor-blading technique were fabricated, the corresponding results are demonstrated in Figure S5 in the Supporting Information. The printed PCDTBT:$PC_{70}BM$ solar cell with hybrid ZnO-PFEP as the CIL exhibits a PCE of 6.26% with a V_{OC} of 0.87 V, a J_{SC} of 10.86 mA cm^{-2}, and a FF of 66%, respectively, which is much higher than that of printed ZnO-based PSCs and comparable to their counterparts prepared with spin-coating technique. Moreover, the performance of the devices with ZnO-PFEP CIL displays high reproducibility, while a large fluctuation in device performance is observed for PSCs with ZnO CIL because of the nonuniform film morphology. This result indicates that the ZnO-PFEP film can serve as a thick CIL to improve the photovoltaic performance, which can be processed with large-area solution processing techniques and potentially be applied in large-area manufacturing of PSCs.

4. CONCLUSIONS

In summary, we report a facile way to fabricate highly conductive and printable cathode interfacial layer for efficient polymer solar cells by sensitizing ZnO nanocrystals with a blue fluorescent conjugated polymer, poly(9, 9-bis (6′-diethoxyl-phosphorylhexyl) fluorene) (PFEP). The PFEP molecules can easily assemble on ZnO NC surfaces through their pending

phosphonate groups and effectively block the aggregation of ZnO NCs, leading to uniform and smooth film during solution processing. Moreover, the conductivity in PFEP sensitized ZnO films is largely improved due to the charge transfer from the PFEP sensitizer driven by electron-chemical potential equilibrium, and such charge-transfer doping effect becomes more pronounced upon illumination due to light excitation of PFEP sensitizer. The increased conductivity in ZnO-PFEP layer renders more efficient electron transport and extraction with respect to pristine ZnO layer. Using ZnO-PFEP as CIL, PSCs with three different polymer donor systems show considerable efficiency enhancements from 44 to 70%. The highest efficiency of 7.56% is achieved in P(IID-DTC):$PC_{70}BM$ based PSCs. These results highlight the feasibility of ZnO-PFEP as a universal CIL to improve the performance of PSCs. Moreover, the enhanced conductivity due to the photo-induced charge-transfer doping effect allows thick ZnO-PFEP film to be used as CIL in large-scale printable PSCs. The printed PCDTBT:$PC_{70}BM$ solar cell with ZnO-PFEP CIL demonstrated a PCE of 6.26% with a FF of 66%, which is comparable to the cell prepared with spin-coating method. This work provides a printable cathode interfacial material that can be potentially applied in large-area manufacturing of PSCs.

■ ASSOCIATED CONTENT

Supporting Information

The energy level alignment diagram of the PCDTBT:$PC_{70}BM$ PSCs with ZnO-PFEP CIL, the illuminated $J-V$ curves of the PSCs with different thicknesses of CILs, optical modeling in a device structure for the PSCs, photovoltaic performance of the PSCs with 120 nm thick PCDTBT:$PC_{70}BM$ active layer combined with 100 nm thick ZnO-PFEP CIL, and experimental data for the PCDTBT:$PC_{70}BM$ PSCs with ZnO and ZnO-PFEP CIL fabricated using doctor-blading technology. This material is available free of charge via the Internet at http://pubs.acs.org.

■ AUTHOR INFORMATION

Corresponding Author

*Tel.: +86 431 8526 2819. Fax: +86 431 8526 2126. E-mail: xiezy_n@ciac.ac.cn.

Notes

The authors declare no competing financial interest.

■ ACKNOWLEDGMENTS

The authors acknowledge the financial support from 973 Project of Ministry of Science and Technology of China (2014CB643504) and the National Natural Science Foundation of China (51325303, 51273193, and 21334006). F.Z. and S.S. acknowledge the financial support from Swedish energy agency (Energimyndigheten).

■ REFERENCES

(1) Blom, P. W. M.; Mihailetchi, V. D.; Koster, L. J. A.; Markov, D. E. Device Physics of Polymer:Fullerene Bulk Heterojunction Solar Cells. *Adv. Mater.* **2007**, *19*, 1551−1566.

(2) Inganas, O.; Zhang, F. L.; Andersson, M. R. Alternating Polyfluorenes Collect Solar Light in Polymer Photovoltaics. *Acc. Chem. Res.* **2009**, *42*, 1731−1739.

(3) Li, G.; Zhu, R.; Yang, Y. Polymer Solar Cells. *Nat. Photonics* **2012**, *6*, 153−161.

(4) Yu, G.; Gao, J.; Hummelen, J. C.; Wudl, F.; Heeger, A. J. Polymer Photovoltaic Cells: Enhanced Efficiencies via a Network of Internal Donor-Acceptor Heterojunctions. *Science* **1995**, *270*, 1789−1791.

(5) Wang, E. G.; Ma, Z. F.; Zhang, Z.; Vandewal, K.; Henriksson, P.; Inganas, O.; Zhang, F. L.; Andersson, M. R. An Easily Accessible Isoindigo-Based Polymer for High-Performance Polymer Solar Cells. *J. Am. Chem. Soc.* **2011**, *133*, 14244−14247.

(6) Liang, Y. Y.; Xu, Z.; Xia, J. B.; Tsai, S. T.; Wu, Y.; Li, G.; Ray, C.; Yu, L. P. For the Bright Future-Bulk Heterojunction Polymer Solar Cells with Power Conversion Efficiency of 7.4%. *Adv. Mater.* **2010**, *22*, E135.

(7) Price, S. C.; Stuart, A. C.; Yang, L. Q.; Zhou, H. X.; You, W. Fluorine Substituted Conjugated Polymer of Medium Band Gap Yields 7% Efficiency in Polymer−Fullerene Solar Cell. *J. Am. Chem. Soc.* **2011**, *133*, 4625−4631.

(8) Li, W.; Hendriks, K. H.; Roelofs, W. S. C.; Kim, Y.; Wienk, M. M.; Janssen, R. A. J. Efficient Small Bandgap Polymer Solar Cells with High Fill Factors for 300 nm Thick Films. *Adv. Mater.* **2013**, *25*, 3182−3186.

(9) Guo, X.; Zhang, M.; Tan, J.; Zhang, S.; Huo, L.; Hu, W.; Li, Y.; Hou, J. Influence of D/A Ratio on Photovoltaic Performance of a Highly Efficient Polymer Solar Cell System. *Adv. Mater.* **2012**, *24*, 6536−6541.

(10) Ye, L.; Zhang, S.; Ma, W.; Fan, B.; Guo, X.; Huang, Y.; Ade, H.; Hou, J. From Binary to Ternary Solvent: Morphology Fine-tuning of D/A Blends in PDPP3T-based Polymer Solar Cells. *Adv. Mater.* **2012**, *24*, 6335−6341.

(11) Yip, H. L.; Jen, A. K. Y. Recent Advances in Solution-processed Interfacial Materials for Efficient and Stable Polymeer Solar Cells. *Energy Environ. Sci.* **2012**, *5*, 5994−6011.

(12) Steim, R.; Kogler, F. R.; Brabec, C. J. Interface Materials for Organic Solar Cells. *J. Mater. Chem.* **2010**, *20*, 2499−2512.

(13) Chen, L.-M.; Xu, Z.; Hong, Z.; Yang, Y. Interface Investigation and Engineering. *J. Mater. Chem.* **2010**, *20*, 2575−2598.

(14) Sondergaard, R.; Helgesen, M.; Jorgensen, M.; Krebs, F. C. Fabrication of Polymer Solar Cells Using Aqueous Processing for All Layers including the Metal Back Electrode. *Adv. Energy Mater.* **2011**, *1*, 68−71.

(15) Sondergaard, R.; Hosel, M.; Angmo, D.; Larsen-Olsen, T. T.; Krebs, F. C. Roll-to-roll Fabrication of Polymer Solar Cells. *Mater. Today* **2012**, *15*, 36−49.

(16) Hau, S. K.; Yip, H. L.; Baek, N. S.; Zou, J. Y.; O'Malley, K.; Jen, A. K. Y. Air-stable Inverted Flexible Polymer Solar Cells Using Zinc Oxide Nanoparticles as an Electron Selective Layer. *Appl. Phys. Lett.* **2008**, *92*, 253301.

(17) Roy, A.; Park, S. H.; Cowan, S.; Tong, M. H.; Cho, S. N.; Lee, K.; Heeger, A. J. Titanium Suboxide as an Optical Spacer in polymer Solar Cells. *Appl. Phys. Lett.* **2009**, *95*, 013302.

(18) Lee, J. H.; Cho, S.; Roy, A.; Jung, H. T.; Heeger, A. J. Enhanced Diode Characteristic of Organic Solar Cells Using Titanium Suboxide Electron Transport Layer. *Appl. Phys. Lett.* **2010**, *96*, 163303.

(19) (a) He, Z.; Zhong, C.; Su, S.; Xu, M.; Wu, H.; Cao, Y. Enhanced Power-conversion Efficiency in Polymer Solar Cells Using an Inverted Device Structure. *Nat. Photonics* **2012**, *6*, 591−595. (b) Zhao, Y.; Xie, Z.; Qin, C.; Qu, Y.; Geng, Y.; Wang, L. Enhanced Charge Collection in Polymer Photovoltaic Cells by Using an Ethanol-soluble Conjugated Polyfluorene as Cathode Buffer Layer. *Sol. Energy Mater. Sol. Cells* **2009**, *93*, 604−608.

(20) Choi, H.; Park, J. S.; Jeong, E.; Kim, G.-H.; Lee, B. R.; Kim, S. O.; Song, M. H.; Woo, H. Y.; Kim, J. Y. Combination of Titanium Oxide and a Conjugated Polyelectrolyte for High-performance Inverted-Type Organic Optoelectronic Devices. *Adv. Mater.* **2011**, *23*, 2759−2763.

(21) Sun, Y.; Seo, J. H.; Takacs, C. J.; Seifter, J.; Heeger, A. J. Inverted Polymer Solar Cells Integrated with a Low-Temperature-Annealed Sol-Gel-Derived ZnO Film as an Electron Transport Layer. *Adv. Mater.* **2011**, *23*, 1679−1683.

(22) Kyaw, A. K. K.; Wang, D. H.; Gupta, V.; Zhang, J.; Chand, S.; Bazan, G. C.; Heeger, A. J. Efficient Solution-Processed Small

Molecule Solar Cells with Inverted Structure. *Adv. Mater.* **2013**, *25*, 2397−2402.
(23) Yang, T.; Wang, M.; Duan, C.; Hu, X.; Huang, L.; Peng, J.; Huang, F.; Gong, X. Inverted Polymer Solar Cells with 8.4% Efficiency by Conjugated Polyelectrolyte. *Energy Environ. Sci.* **2012**, *5*, 8208−8214.
(24) Chen, S.; Small, C. E.; Amb, C. M.; Subbiah, J.; Lai, T.-h.; Tsang, S.-W.; Manders, J. R.; Reynolds, J. R.; So, F. Inverted Polymer Solar Cells with Reduced Interface Recombination. *Adv. Energy Mater.* **2012**, *2*, 1333−1337.
(25) Beek, W. J. E.; Wienk, M. M.; Kemerink, M.; Yang, X. N.; Janssen, R. A. J. Hybrid Zinc Oxide Conjugated Polymer Bulk Heterojunction Solar Cells. *J. Phys. Chem. B* **2005**, *109*, 9505−9516.
(26) Hau, S. K.; Yip, H.-L.; Ma, H.; Jen, A. K. Y. Broadband Electro-optic Polymer Modulators with High Electro-optic Activity and Low Poling Induced Optical Loss. *Appl. Phys. Lett.* **2008**, *93*, 043507.
(27) Small, C. E.; Chen, S.; Subbiah, J.; Amb, C. M.; Tsang, S. W.; Lai, T. H.; Reynolds, J. R.; So, F. High-Efficiency Inverted Dithienogermole-Thienopyrrolodione-Based Polymer Solar Cells. *Nat. Photonics* **2012**, *6*, 115−120.
(28) Stubhan, T.; Oh, H.; Pinna, L.; Krantz, J.; Litzov, I.; Brabec, C. J. Inverted Organic Solar Cells Using a Solution Processed Aluminum-Doped Zinc Oxide Buffer Layer. *Org. Electron.* **2011**, *12*, 1539−1543.
(29) Stubhan, T.; Krantz, J.; Li, N.; Guo, F.; Litzov, I.; Steidl, M.; Richter, M.; Matt, G. J.; C. Brabec, J. High Fill Factor Polymer Solar Cells Comprising a Transparent, Low Temperature Solution Processed Doped Metal Oxide/Metal Nanowire Composite Electrode. *Sol. Energy Mater. Sol. Cells* **2012**, *107*, 248−251.
(30) Savva, A.; Choulis, S. A. Cesium-Doped Zinc Oxide as Electron Selective Contact in Inverted Organic Photovoltaics. *Appl. Phys. Lett.* **2013**, *102*, 233301.
(31) Zhou, G.; Qian, G.; Ma, L.; Cheng, Y. X.; Xie, Z. Y.; Wang, L. X.; Jing, X. B.; Wang, F. S. Polyfluorenes with Phosphonate Groups in the Side Chains as Chemosensors and Electroluminescent Materials. *Macromolecules* **2005**, *38*, 5416−5424.
(32) Mihailetchi, V. D.; Xie, H. X.; deBoer, B.; Koster, L. J. A.; Blom, P. W. M. Charge Transport and Photocurrent Generation in Poly(3-hexylthiophene): Methanofullerene Bulk-Heterojunction Solar Cells. *Adv. Funct. Mater.* **2006**, *16*, 699−708.
(33) Zhang, B. H.; Qin, C. J.; Ding, J. Q.; Chen, L.; Xie, Z. Y.; Cheng, Y. X.; Wang, L. X. High-Performance All-Polymer White-Light-Emitting Diodes Using Polyfluorene Containing Phosphonate Groups as an Efficient Electron-Injection Layer. *Adv. Funct. Mater.* **2010**, *20*, 2951−2957.
(34) Liu, J.; Shao, S. Y.; Meng, B.; Fang, G.; Xie, Z. Y.; Wang, L. X.; Li, X. L. Enhancement of Inverted Polymer Solar Cells with Solution-Processed ZnO-TiOx Composite as Cathode Buffer Layer. *Appl. Phys. Lett.* **2012**, *100*, 213906.
(35) Chen, S. H.; Su, A. C.; Su, C. H.; Chen, S. A. Crystalline Forms and Emission Behavior of Poly(9,9-di-n-octyl-2,7-fluorene). *Macromolecules* **5**, *38*, 379−385.
(36) Chen, X.; Wan, H.; Li, H. D.; Cheng, F. M.; Ding, J. Q.; Yao, B.; Xie, Z. Y.; Wang, L. X.; Zhang, J. D. Influence of Thermal Annealing Temperature on Electro-Optical Properties of Polyoctylfluorene Thin Film: Enhancement of Luminescence by Self-Doping Effect of Low-Content Phase Crystallites. *Polymer* **2012**, *53*, 3827−3832.
(37) Talapin, D. V.; Lee, J. S.; Kovalenko, M. V.; Shevchenko, E. V. Prospects of Colloidal Nanocrystals for Electronic and Optoelectronic Applications. *Chem. Rev.* **2010**, *110*, 389−458.
(38) Tang, J. A.; Sargent, E. H. Infrared Colloidal Quantum Dots for Photovotaics: Fundamentals and Recent Progress. *Adv. Mater.* **2011**, *23*, 12−29.
(39) Lampert, M. A.; Mark, P. *Current Injection in Solids*; Academic Press: New York, 1973.
(40) Chiguvare, Z.; Dyakonov, V. Trap-Limited Hole Mobility in Semiconducting Poly(3 hexylthiophene). *Phys. Rev. B* **2004**, *70*, 235207.
(41) Shao, S.; Liu, J.; Zhang, B.; Xie, Z.; Wang, L. Enhanced Stability of Zinc Oxide-Based Hybrid Polymer Solar Cells by Manipulating Ultraviolet Light Distribution in the Active Layer. *Appl. Phys. Lett.* **2011**, *98*, 203304.
(42) Bhat, S. V.; Vivekchand, S. R. C.; Govindaraj, A.; Rao, C. N. R. Photoluminescence and Photoconducting Properties of ZnO. *Solid State Commun.* **2009**, *149*, 510−514.
(43) Sharma, S. K.; Pujari, P. K.; Sudarshan, K.; Dutta, D.; Mahapatra, M.; Godbole, S. V.; Jayakumar, O. D.; Tyagi, A. K. Positron Annihilation Studies in ZnO Nanoparticles. *Solid State Commun.* **2009**, *149*, 550−554.
(44) Sista, S.; Park, M.-H.; Hong, Z.; Wu, Y.; Hou, J.; Kwan, W. L.; Li, G.; Yang, Y. Highly Efficient Tandem Photovoltaic Cells. *Adv. Mater.* **2010**, *22*, 380−383.
(45) Walzer, K.; Maennig, B.; Pfeiffer, M.; Leo, K. Highly Efficient Organic Devices Based on Electrically Doped Transport Layers. *Chem. Rev.* **2007**, *107*, 1233−1271.
(46) Shao, S.; Zheng, K.; Pullerits, T.; Zhang, F. Enhanced Performance of Inverted Solar Cells Using Poly(ethylene oxide) Modified ZnO as Cathode Buffer Layer. *ACS Appl. Mater. Interfaces* **2013**, *5*, 380−385.
(47) Greiner, M. T.; Helander, M. G.; Tang, W.-M.; Wang, Z.-B.; Qiu, J.; Lu, Z.-H. Universal Energy-Level Alignment of Molecules on Metal Oxides. *Nat. Mater.* **2012**, *11*, 76−81.
(48) Qi, B. Y.; Wang, J. Z. Fill Factor in Polymer Solar Cells. *Phys. Chem. Chem. Phys.* **2013**, *15*, 8972−8982.
(49) Chen, B. B.; Qiao, X. F.; Liu, C. M.; Zhao, C.; Chen, H. C.; Wei, K. H.; Hu, B. Effects of Bulk and Interfacial Charge Accumulation on Fill Factor in Organic Solar Cells. *Appl. Phys. Lett.* **2013**, *102*, 193302.